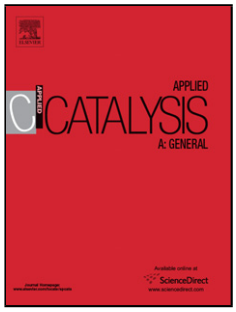

Title: Atomically Precise Ag nanoclusters Intercalated in Zirconium Pyrophosphate for Efficient Hydrogenation of Nitroaromatics

Authors: Honghui Gong, Lina Lin, Xiuge Zhao, Huan Li, Difan Li, Zichen Xu, Manyu Chen, Rong Huang, Zhenshan Hou

PII: S0926-860X(19)30034-1
DOI: https://doi.org/10.1016/j.apcata.2019.01.018
Reference: APCATA 16958

To appear in: *Applied Catalysis A: General*

Received date: 12 November 2018
Revised date: 20 January 2019
Accepted date: 24 January 2019

Please cite this article as: Gong H, Lin L, Zhao X, Li H, Li D, Xu Z, Chen M, Huang R, Hou Z, Atomically Precise Ag nanoclusters Intercalated in Zirconium Pyrophosphate for Efficient Hydrogenation of Nitroaromatics, *Applied Catalysis A, General* (2019), https://doi.org/10.1016/j.apcata.2019.01.018

Atomically Precise Ag nanoclusters Intercalated in Zirconium Pyrophosphate for Efficient Hydrogenation of Nitroaromatics

Honghui Gong,[a] Lina Lin,[c] Xiuge Zhao,[a] Huan Li, [b,*] Difan Li,[a] Zichen Xu,[a] Manyu Chen,[a] Rong Huang, [c,*] Zhenshan Hou[a,*]

[a]*Key Laboratory for Advanced Materials, School of Chemistry and Molecular Engineering, East China University of Science and Technology, Shanghai 200237, China. E-mail: houzhenshan@ecust.edu.cn.*
[b]*Institute of Crystalline Materials, Shanxi University, Taiyuan 030006, Shanxi, China.*
[c]*Key Laboratory of Polar Materials and Devices, Ministry of Education, East China Normal University, Shanghai 200062, China.*

[*]*Corresponding author. E-mail address: houzhenshan@ecust.edu.cn (Z. Hou).*

Graphical abstract

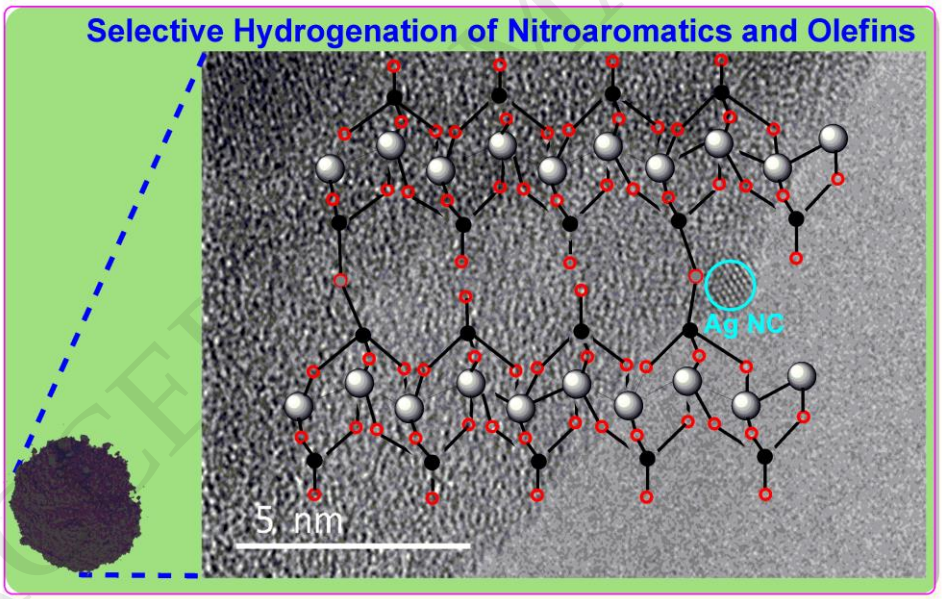

Highlights

- Atomically precise Ag nanoclusters was intercalated in zirconium

pyrophosphate.

- The residual carbon on Ag cluster was very crucial for protecting Ag nanocluster from sintering.
- The resulting material was highly efficient for catalytic hydrogenation.
- The Ag catalyst showed excellent recyclability in hydrogenation reaction.

Abstract: Designing and fabricating catalysts with highly dispersed metal nanoclusters (NCs) is very crucial for achieving high activity and selectivity. In this work, all-alkynyl-protected $[Ag_{74}(C{\equiv}CPh)_{44}](NO_3)_2$ cluster (Ag cluster) with a well-defined structure was firstly intercalated in α-zirconium phosphate (α-ZrP) through ion-exchange. Then the atomically precise Ag cluster can be immobilized robustly in the support by a sequential process of carbonization, calcination and reduction. The supported Ag cluster showed the relatively high catalytic activity (TOF=222.9-445.8 h^{-1}) and excellent recyclability for hydrogenation of a variety of nitroaromatics, as well as the compounds with carbon-carbon double bonds even if the loading of Ag was as low as 0.72 wt.%. Zirconium pyrophosphate acts as not only a stabilizer of Ag cluster through a spatial confinement, but also an adsorption site for nitroaromatics. The residual carbon arisen from thermal decomposition of all-alkynyl ligand coordinating on Ag cluster exerted an important role in protecting Ag cluster from sintering. As a result, the intercalation of Ag cluster in the interlayer region is a promising strategy for extending their potential applications in catalysis.

Keywords: Ag nanocluster; Zirconium phosphate; Intercalation; Carbonization; Hydrogenation of nitroaromatics.

1. Introduction

Heterogeneous catalysts with metal NCs as active centers occupy an extremely important position in basic research and chemical industry, considering that metal NCs (1–2 nm) exhibit high specific surface area, unique core-shell structures and

specific electronic properties which make them a unique class of catalysts [1–3]. However, the traditional preparation methods are difficult to obtain NCs with uniform size and composition, and this shortcoming brings great difficulties to the regulation of catalyst selectivity and activity, let alone the study of catalytic mechanism [4]. Great progress has been made in the study of nano-metal clusters with precise composition and structure recently, creating a rare opportunity to solve this problem [5]. However, how to load uniformly these metal NCs on a suitable support to maximize their catalytic efficiency and ensure the stability of these NCs under the reaction conditions is still a challenging research topic [6].

Zirconium phosphates (ZrP) are multifunctional materials, which are useful in many industrial and advanced scientific applications such as proton conducting membrane, ion-exchange, adsorbent and as substrate for immobilization of biological materials [7,8]. Among the ZrP materials, α-ZrP is the most widely investigated and used in catalysis because it possess trenchant plates, the thin plates of α-ZrP were almost identical and the solid layers are placed in parallel in addition to strong ion-exchange [9,10]. In recent years, more and more researchers have utilized the ion-exchange properties of α-ZrP to optimize its applications in catalysis. For examples, α-ZrP has been modified by introducing inorganic or organic compounds into ZrP matrix, especially intercalating with metal ions, small organic groups and even polymers, would bring unexpected active sites for specific catalytic reactions [11,12]. With regard to the stabilization of the metal NCs on a solid support, in this work we have developed a new approach to intercalate atomically precise Ag cluster into α-ZrP matrix by ion exchange. As we have known, most of the reported silver nanoscale clusters are protected by thiol ligands, while sulfur-containing compounds usually cause the catalyst poisoning [13]. Therefore, in this work an allalkynyl-protected cation Ag cluster ($[Ag_{74}(C{\equiv}CPh)_{44}](NO_3)_2$) has been used as catalyst precursor [14]. More importantly, the surface carbon ligand plays a crucial role in improving the stability of the Ag cluster in the course of the thermal treatment. Aromatic amines are important raw materials and industrial intermediates, which are widely used for the synthesis of pharmaceuticals, medicine, dyes, polymers and other

fine chemicals [15].

Catalytic hydrogenation of nitroaromatics is an environmental benign route for the production of aromatic amines [16]. The noble metal heterogeneous catalysts (Pt, Au, Pd, Ru etc.) usually possess high catalytic activity in hydrogenation of nitroaromatics, but they are very expensive for practical uses and sometimes lack chemoselectivity [17–19]. Silver has been realized as the highly selective hydrogenation catalysts and received more and more attentions in recent years, which have also the advantages over platinum-group metal catalysts in that silver acts as a less expensive group IB metal [20]. In this work, we have intercalated the atomically precise Ag cluster into α-ZrP and the resultant material was employed as a catalyst for selective hydrogenation of nitroaromatics and olefins to the corresponding products. It was found that the resulting Ag catalyst possessed not only high catalytic activity and selectivity, but also excellent stability for hydrogenation of nitroaromatics.

2. Experimental

2.1. Materials

Zirconium oxychloride, ammonium dihydrogen phosphate, silver nitrate, tetrahydrofuran (THF), 1, 3-bis(diphenylphosphino) propane (dppp), phenylacetylene, sodium borohydride, N,N-Dimethylformamide (DMF), anhydrous ethanol, dichloromethane were purchased from Sino pharm Chemical Reagent Co. Ltd. (Shanghai, China). High purity N_2 (99.999%) and H_2 (99.999%) was supplied by Shang Nong Gas Factory. All other chemicals (analytical grade) were from Sino pharm Chemical Reagent Co. Ltd and used as received without any further purification.

2.2. Catalyst preparation

2.2.1. Preparation of α-ZrP

α-ZrP was synthesized according to the classical refluxing method [21]. Briefly, 10.0 g $ZrOCl_2 \cdot 8H_2O$ was refluxed with 100.0 mL 6.0 M H_3PO_4 in a Pyrex glass flask at 100 °C for 24 h. After that, the products were washed a few times until the pH=7

and collected by centrifugation. Then, the products were dried at 65 °C for 24 h in oven. The dried α-ZrP was ground with a mortar and pestle into fine white powders. The final products were identified as α-ZrP.

2.2.2. Preparation of the Ag cluster ($[Ag_{74}(C{\equiv}CPh)_{44}](NO_3)_2$)

The Ag cluster was prepared according to our previously published procedure [14]. 10 mg $AgNO_3$ was dissolved in 2 mL ethanol, then 8 μL phenylacetylene and 25 mg 1, 3-bis(diphenyphosphino) propane dissolved in 2 mL CH_2Cl_2 were added under vigorous stirring. After that, added the freshly prepared solution of $NaBH_4$ (0.1 mmol in 400 μL ethanol). The solution changed from colorless to light yellow. The reaction was aged for 12 h at ambient conditions, during which the color further turned dark brown red. The mixture was evaporated to dryness to give a dark solid, which was dissolved in CH_2Cl_2 (2 mL) and centrifuged for 5 min at 12000 r/min. The supernatant solution was evaporated to dryness to give a dark solid, which was identified as $[Ag_{74}(C{\equiv}CPh)_{44}](NO_3)_2$.

2.2.3. Preparation of the Ag catalyst

0.5 g α-ZrP was dispersed in 30 mL DMF under ultrasonic vibration for 30 minutes. Subsequently, 7.5 mg $[Ag_{74}(C{\equiv}CPh)_{44}](NO_3)_2$ was dissolved in 20 mL DMF and then added dropwise to the above suspension at 100 °C under vigorous stirring. After 5 h, the suspension was centrifuged and then the isolated solid was dried under the vacuum at 80 °C for 4 h. The obtained white powder was named as Ag/α-ZrP, which was then carbonized at 750 °C (2 °C/min) for 3 h under N_2 flow. In this step, it was found that α-ZrP was transformed into zirconium pyrophosphate (ZrPP) due to the condensation of P-OH groups. The resulting material was designated as Ag@C/ZrPP, followed by calcining at 500 °C for 1 h in a muffle furnace to give Ag@C/ZrPP-500. Next, Ag@C/ZrPP-500 was reduced at 300 °C for 2 h under 10% H_2 in N_2 to afford Ag@C/ZrPP-500R catalyst. The actual content of Ag was found to be 0.72 wt.% via inductively coupled plasma atom emission spectroscopy (ICP-AES).

2.3. Catalyst characterization

X-ray diffraction (XRD) analysis of types samples were performed in the 2θ range of 10°-80° on an Rigaku D/MAX 2550 VB/PC instrument using a graphite crystal a monochromator. The textural properties from N_2 adsorption isotherms were obtained on Quanta chrome NOVA 2200e equipment. The surface area was obtained from the isotherms in the relative pressure range of 0.0~0.35. Pore volume was determined at p/p_0 of 0.99. The inductively coupled plasmaatomic emission spectroscopy (ICP-AES) analysis was carried out on a Varian ICP-710ES instrument. The sample was putted in a plastic beaker mixed with a certain amount of aqua regia and HF at 120 °C for 4h to dissolve the sample easily, followed by diluted with water. FT-IR spectra were recorded from pressed KBr pellets at room temperature on a Nicolet Fourier transform infrared spectrometer (Magna550). A spectrum of dry KBr was also recorded as background. The FT-IR spectra of the Ag catalysts after introducing nitrobenzene (3.0 mmol g^{-1}) was carried out according to the following procedure: a mixture of nitroaromatics (0.3 mmol), THF (1.0 mL) and the catalysts (0.1 g) were placed in a 25.0 mL Schlenk flask and stirred for 1 h, followed by drying under the vacuum for 1 h at 40 ^{o}C. The resulting sample was subjected to FT-IR measurement. The thermal stability of catalysts was determined by Thermogravimetry analysis (TGA) method (heating rate: 10 $^{o}C \cdot min^{-1}$; air flow, 100 $mL \cdot min^{-1}$) using PerkinElmerPyris Diamond Analyser. The scanning electron microscopy (SEM) images were performed on JSM electron microscopes. HRTEM was performed in a JEOL JEM-2100F transmission electron microscope operating at 200 kV with a nominal resolution of 0.25 nm. The samples for TEM were prepared by dropping the aqueous solutions containing the nanoparticles onto the carbon-coated Cu grids. The high angle annular dark field scanning transmission electron microscopy (HAADF-STEM) was analyzed using the FEI Tecnai G^2 F20 TEM. Temperature-programmed reduction (H_2-TPR) was performed using VDsorb-91i. The catalyst was placed in a ushaped quartz tube, then purged under pure Ar (10 cm^3 min^{-1}) flow at 400 °C for 1 h, and then cooled down to 20 °C. After that, it was reduced with H_2/Ar (10/90, vol/vol) (10 mL min^{-1}) up to 500 °C (ramp rate of 10 °C min^{-1}). Raman spectroscopy was performed using a

Thermo Scientific DXR Raman microscope, and X-ray photoelectron spectroscopy (XPS) was performed using (Thermo ESCALAB 250). ^{1}H NMR spectra were recorded on a Bruker AVANCE 400 MHz instrument (400 MHz ^{1}H NMR) using $CDCl_3$ or $(CD_3)_2SO$ as solvent and TMS as the reference, respectively. The solid-state ^{31}P MAS NMR spectra were performed with a VNMRS400WB spectrometer (162 MHz for ^{31}P nuclei) equipped with a standard 4 mm MAS NMR probe head. The ^{31}P chemical shifts were referred to H_3PO_4.

2.4. Typical procedure for the hydrogenation of nitroaromatics

The hydrogenation of nitroaromatics was carried out as follows. The mixture of nitroaromatics (1.5 mmol), THF (5.0 mL) and the Ag@C/ZrPP-500R catalyst (0.05 g) were placed in a 25 mL Schlenk flask equipped with a magnetic stirrer and purged five times with N_2 to replace the air in the autoclave, five times with pure H_2 to replace the N_2 prior to experiments. Finally, hydrogen was added to the given pressure and the reactor was heated to 160 °C with vigorous stirring. After the hydrogenation reactions, the Schlenk flask was cooled quickly to room temperature. Then the catalyst was filtrated to separate from the solution, the filtrate was added to the volumetric flask and the catalyst was washed with THF and dried at 40 °C overnight and used for the next run. The liquid products were analyzed by Shimadzu GC-2014 equipped with an KB-50 MS (30 m long, 0.32 mm i.d., 0.50 μm film thickness) and an Agilent 6890/5973 GC-MS system equipped with a HP-5MS column (30 m long, 0.25 mm i.d., 0.25 μm film thickness). The obtained products were isolated and purified by evaporation or column chromatography, and then analyzed by ^{1}H NMR (Fig. S6-S14).

3. Results and Discussion

We firstly prepared the cationic Ag cluster and employed the cluster as the catalyst precursor. The thermal stability of Ag cluster was investigated in the range of 50 to 800 °C by TGA. It can be found that there are two sharp thermal weight loss: the first is between 150 °C and 300 °C (*ca.*14%), which mainly corresponded to the initial

decomposition, and the other appears between 300 °C and 700 °C (*ca.*16%) likely due to the removal of ligands tethered more tightly to Ag cluster (Fig. S1). This result demonstrates that the weight content of the surface ligands is determined as about 30% by thermogravimetric analysis, which is consistent with that of its molecular structure. The cationic Ag cluster is intercalated easily into the interlayer region of α-ZrP by ionic-exchange to afford Ag/α-ZrP. Next, the resultant material Ag/α-ZrP undergoes a sequential process of the carbonization, calcination and reduction to afford the corresponding Ag@C/ZrPP, Ag@C/ZrPP-500, Ag@C/ZrPP-500R catalysts, respectively (Scheme 1). The surface ligands can be converted into carbon layer on Ag cluster during the course of the subsequent thermal treatment.

<Insert Scheme 1>

The porosity properties of the different catalysts were determined by N_2 adsorption-desorption analysis. The corresponding specific porosity datas are listed in Table 1. The pore size distribution presents typical mesopores in all samples shown in Table 1, ranging from 10.5 nm to 12.0 nm. The total surface area calculated by the BET method and pore volume of the Ag/α-ZrP show a slight decrease, compared with that of α-ZrP (Table 1, entries 1 and 2), which reflects that the Ag clusters could be introduced to the interlayers of α-ZrP. In consideration of Ag@C/ZrPP, Ag@C/ZrPP-500 and Ag@C/ZrPP-500R catalysts, the BET surface area, total pore volume and the pore size almost show no changes compared with that of Ag/α-ZrP (Table 1, entries 2-5). This reveals that the porous properties do not undergo any changes even if the Ag/α-ZrP is subjected to a sequential thermal treatment under high temperature.

<Insert Table 1>

Fig. 1 shows the XRD patterns of all catalysts. The XRD patterns of the α-ZrP (Fig. 1a) display three main strong diffraction peaks at 11.7°, 19.8° and 24.9°, corresponding to the (002), (110) and (112) planes, respectively. These three

diffraction planes are in accordance with monoclinic structure with space group $P2_1/n$ [21]. After the introduction of Ag cluster into α-ZrP, the pattern of Ag/α-ZrP catalyst shows a strong diffraction peak shifted from 11.7° to 7.9° (Fig. 1b). As compared with that of α-ZrP, the peak is moved to lower angle. This means that the interlayer spacing of α-ZrP in Ag/α-ZrP catalyst becomes more wide (up to *ca.* 1.12 nm) due to the intercalation of the partial Ag clusters into the interlayers of α-ZrP [22]. Interestingly, after the Ag/α-ZrP catalyst is subjected to thermal treatment, the resulting materials Ag@C/ZrPP, Ag@C/ZrPP-500 and Ag@C/ZrPP-500R show no diffraction peaks corresponding to the α-ZrP. The four new weak diffraction peaks appear at 14.5°, 21.6°, 24.09° and 33.8° (JCPDS 36-0188) (Fig. 1c-1e), corresponding to zirconium pyrophosphate (ZrPP) although the crystallinity of the resulting ZrPP is poor under high temperature treatment [23]. It should be noted that no any diffraction peaks corresponding Ag species in all catalysts was observed in Fig. 1, indicating that the Ag particles existed in a very small size or high dispersion.

< Insert Fig. 1>

Fig. 2 shows the FT-IR spectra of the Ag catalysts. Vibrations corresponding to P-O stretching vibration are located between 1000 and 1100 cm^{-1}. The absorption band at 1622 cm^{-1} belongs to the bending vibration absorption of water in all samples and strong absorption band at 3155 cm^{-1} belongs to the PO-H vibration band. Additionally, the two sharp absorption bands around 3595 and 3510 cm^{-1} are the characteristic peaks of water asymmetric and symmetric stretching vibration absorption (Fig. 2a and 2b) [24]. It can be clearly seen that when the catalysts are subjected to thermal treatment (Fig. 2c-2e), a new peak appears at 755 cm^{-1}, which is assigned to the P-O-P deforming vibration (poly phosphate), indicating that P-O-P bond could be generated from the P-OH in α-ZrP by condensation under high temperature, being consistent with the results of XRD patterns (Fig. 1c-1e). While the band at 530 cm^{-1} also appears in all samples due to the (P)-O-H deformation vibration (Fig. 2a-2e). The results demonstrate that both (P)-O-H and P-O-P are present even if

the ZrP undergoes high temperature treatment. The bands around 1000-1100 cm^{-1} corresponding to the P-O stretching vibration are shifted towards higher wavenumbers by 50 cm^{-1} (from 1045 cm^{-1} to 1095 cm^{-1}), indicating that the P-O bonds in the tetrahedral become more covalent after thermal treatment. The bands at 3433 cm^{-1} are attributed to the OH asymmetric stretching vibration. The absorption bands at 1622, 3510 and 3595 cm^{-1} resulting from water stretching vibration disappeared or weaken imply that the water is basically removed due to thermal treatment (Fig. 2c-2e) [25].

< Insert Fig. 2>

Solid-state ^{31}P MAS NMR spectra of the ZrP-based samples were performed to evaluate the coordination state of the phosphorous atoms. As shown in Fig. 3a, the spectra of the α-ZrP show the single peak at -20 ppm, which can be attributed to the presence of $[(OH)P\text{-}(OZr)_3]$. There is only one signal at -23 ppm in the ^{31}P MAS NMR spectra of the Ag/α-ZrP catalyst (Fig. 3b), which might reflect the change of the ionization state of the phosphate due to the substitution of the proton in $[(OH)P\text{-}(OZr)_3]$ groups by $[Ag_{74}(C{\equiv}CPh)_{44}]^{2+}$ cations. Furthermore, the Ag@C/ZrPP-500R catalyst shows a low intense peak appeared at -33 ppm, as compared with that of Ag/α-ZrP catalyst (Fig. 3c). This can be attributed to the presence of polyphosphate (P-O-P) bond [26-28], being consistent with the characterization of both FT-IR and XRD.

< Insert Fig. 3>

Based on the above characterization of porosity, XRD, FT-IR and ^{31}P MAS NMR, it indicates that the cationic Ag cluster has been partially intercalated into the interlayers of α-ZrP through ion exchange and the α-ZrP is transformed into ZrPP under high temperatures. However, the nature of the resulting Ag particles supported on ZrPP is still not clear. Subsequently, the surface morphology of the catalysts was examined by SEM. As shown in Fig. 4a, α-ZrP shows many trenchant plates in which

the disks have well-defined shapes with very smooth surface. The thin plates of α-ZrP are almost identical and the solid layers are placed in parallel, showing good crystallinity. It could be seen from Fig. 4b that the Ag/α-ZrP material shows as the same layered structure as that of α- ZrP, indicating there is no change in surface morphology after intercalation of the cationic Ag cluster. More interestingly, the resultant Ag@C/ZrPP, Ag@C/ZrPP-500 and Ag@C/ZrPP-500R catalysts show also no obvious changes in the surface morphology, as compared with α-ZrP, demonstrating that the catalysts still possess a similar layered structure and a comparable texture inherit from the α-ZrP structure (Fig. 4c-e).

< Insert Fig. 4>

The HRTEM images of the Ag_{74} cluster precursor have been showed in Fig. 5a and 5b. It can be seen that the mean size of the Ag cluster precursor is about 1.35 nm (sizes mainly ranging from 1-2 nm) (Fig. 5a), and Ag cluster is highly dispersed prior to immobilization. As shown in Fig. 5c, the Ag@C/ZrPP-500R catalyst displays many small and regular nanoplate-like structure particles. The resulting Ag cluster is intercalated in ZrPP and exhibits a very small mean size (1.43 nm) mainly ranging from 1 nm to 2 nm (Fig. 5c), which evidences that the Ag cluster remains almost the same size as that of Ag cluster precursor even after the multistep thermal treatment. Fig. 5d shows the HRTEM image of the Ag@C/ZrPP-500R with a higher magnification, in which the lattice fringes can be observed clearly, indicating the crystalline nature of the Ag clusters displaying a face-centered cubic (fcc) structure. Application of Fast Fourier Transformation (FFT) treatment to this image showed reflections corresponding to the fcc-Ag (111) atomic planes with typical lattice separations of 0.235 nm [29]. Additionally, the nanostructure and morphology of the Ag cluster are imaged by HAADF-STEM images (Fig. 5e and 5f, white dots). The Ag clusters with a mean size of 1-2 nm are discernable, suggesting that the Ag cluster is well dispersed without aggregation during the procedure.

< Insert Fig. 5>

The redox properties of the catalysts were investigated by H_2-TPR as shown in Fig. S2. All the TPR profiles appear in the temperature range of 50-500 °C. The ZrPP sample exhibit no peaks, indicating ZrPP cannot be reduced in the temperature range of 50-500 °C (Fig. S2a). There are also no peaks observed in Ag@C/ZrPP sample, which means that the Ag species in the Ag@C/ZrPP maintain in the reduced state (Fig. S2b). The temperature peak is observed only for Ag@C/ZrPP-500 sample presents at 267 °C, corresponding to the reduction of Ag_2O to metallic Ag (Fig. S2c) [30].

Next, the chemical state of Ag species in ZrPP was characterized by XPS. Fig. 6 shows the XPS survey spectra of Ag@C/ZrPP-500R catalyst. As shown in the narrow scan spectrum of Ag 3d (Fig. 6), the two peaks around 368.0 and 374.1 eV could be ascribed to Ag $3d_{5/2}$ and Ag $3d_{3/2}$ [31], respectively, which are the typical binding energy of metallic Ag, being consistent with that of H_2-TPR characterization.

< Insert Fig. 6>

The Raman spectra have been performed to identify the role of the residual carbon remained on the surface of the Ag catalyst during the course of thermal treatment (Fig.7). There is no peak range from 1000 cm^{-1} to 2000 cm^{-1} for the ZrPP (Fig. 7a). Both Ag@C/ZrPP and Ag@C/ZrPP-500R catalysts show two major peaks around 1346 cm^{-1} and 1573 cm^{-1}. The peak at 1573 cm^{-1} represents graphitic, designated as G-band and the peak at 1346 cm^{-1} is attributed to defects present in the structural units of graphite, designated as D-band (Fig.7b and 7c) [32], indicating that calcination in air at 500 °C does not remove the carbon completely on the Ag particles surface. However, no peaks appear around 1346 cm^{-1} and 1573 cm^{-1} on Ag@C/ZrPP-550R catalyst. Therefore, the calcination under higher temperature (550 °C) indeed can remove the carbon layer completely on the surface of Ag cluster (Fig. 7d).

< Insert Fig. 7>

4. Catalytic hydrogenation of nitroaromatics

The hydrogenation of nitrobenzene was initially adopted as a model reaction to evaluate the activity and selectivity for the different catalysts. As shown in Table 2, it can be seen that the hydrogenation of nitrobenzene cannot happen without catalyst (Table 2, entry 1), and Ag cluster precursor as a catalyst gives the poor conversion (5%). After the reaction, the black particles are visually precipitated, indicating that the Ag cluster is unstable at 160 °C (Table 2, entry 2). It is observed that both α-ZrP and ZrPP catalysts afforded no activity for nitrobenzene hydrogenation (Table 2, entries 3 and 4), indicating that they are unable to catalyze nitrobenzene conversion. The Ag/α-ZrP catalyst shows only 7.5% conversion of nitrobenzene, which reveals that α-ZrP supporting Ag cluster actually shows very low activity for nitrobenzene hydrogenation likely because organic ligands block the catalytically active sites (Table 2, entry 5). Similarly, the Ag@C/ZrPP catalyst gives no activity probably due to the thick carbonaceous layers, which cover the surface of Ag particles, resulting in the poor activity (Table 2, entry 6). To our great delight, once the partial carbon layer on the surface of Ag cluster is removed partially at 400°C, followed by reducing with H_2, the resulting catalyst Ag@C/ZrPP-400R shows a significant increase of the conversion, which can reach to 67.5% (Table 2, entry 7). Furthermore, when the Ag catalyst is subjected to calcination at high temperature (500°C), the resulting Ag@C/ZrPP-500R could give full conversion of nitrobenzene (Table 2, entry 8). It demonstrates that partially removing carbon layer on the surface of Ag cluster could allow the catalyst to expose more active sites and thus enhance the catalytic performance (Table 2, entries 7 and 8). However, if the Ag catalyst is calcined at 550° (Ag@C/ZrPP-550R), the carbon layer is fully removed (Fig. 7d), and the nitrobenzene conversion decreases sharply to 44.5% in this case (Table 2, entry 9). As shown in HRTEM images (Fig. S3), the full removal of carbon layer can lead to the serious agglomeration and sintering of Ag cluster, which could account for an obvious decease of catalytic activity (Table 2, entry 9). As a result, the presence of the partial carbon layer is very important for stabilization and dispersion of Ag cluster.

<Insert Table 2>

Since Ag@C/ZrPP-500R catalyst showed excellent activity for hydrogenation of nitrobenzene, it was employed as the catalyst to investigate the effect of different reaction temperatures on the activity. It can be seen that the reaction temperature has a significant influence on the hydrogenation of nitrobenzene as shown in Fig. S4. At 130 °C, the conversion of nitrobenzene is only 48%. At 140 °C, the conversion of nitrobenzene is 69%. Nitrobenzene conversion increases to 85% with the reaction temperature rises up to 150 °C. When the reaction temperature is above 160 °C, the full conversion of nitrobenzene is achieved and the yield of aniline reaches to 100%. In all cases, only aniline is detected as a sole product.

The reaction kinetics of nitrobenzene hydrogenation under the different reaction temperatures were investigated accordingly. It has been reported that the substrate (nitrobenzene) could be assumed to meet the first-order kinetics in nitrobenzene hydrogenation since H_2 is existed in a great excess (4.0 MPa H_2) [33]. Hence, the activation energy of nitrobenzene hydrogenation over Ag@C/ZrPP-500R catalyst can be deduced from Fig. 8 in the temperature range of 140-170 °C and it is as low as 46.33 kJ mol^{-1}, accounting for the higher hydrogenation activity. This illustrates that the present Ag catalyst exhibits relatively low activation energy for nitrobenzene hydrogenation, as compared with that of the previous reports (26 to 67 kJ mol^{-1}) [34].

< Insert Fig. 8>

Inspired by the high catalytic performance of Ag@C/ZrPP-500R, under optimal conditions, we subsequently examined the substrate scope with a wide range of the other important nitroaromatics. A variety of nitroaromatics were smoothly hydrogenated with high reactivities and yields using the present Ag@C/ZrPP-500R catalyst (Table 3). It is well known that the dehalogenation of halogen-substituted nitroaromatics is a serious issue in the selective hydrogenation. To our great delight,

the 4-nitrochlorobenzene is completely converted and reduced to corresponding chloro-aniline with excellent yield of 99.5% (Table 3, entry 2). Furthermore, an excellent catalytic performance is also obtained in the reduction of methyl-, hydroxyl-, and methoxy-substituted nitroaromatics (Table 3, entries 3-6) as well as amino nitroarene (Table 3, entry 7) without detectable by-products. Especially, the selective hydrogenation of the nitro groups in the benzene ring with reducible functional groups (acetyl group) also give >94% yield to the corresponding amines (Table 3, entries 8 and 9), further highlighting that the developed Ag@C/ZrPP-500R catalyst acts as a promising candidate for production of aromatic amines via highly selective hydrogenation from their corresponding nitroaromatics. It is illustrated that the Ag@C/ZrPP-500R catalyst could smoothly catalyze each functional nitroaromatics fully, and exhibits outstanding selectivity to the corresponding aromatic amines. To the best of our knowledge, the Ag@C/ZrPP-500R catalyst shows 2 to 15 times higher turnover frequency (TOF=222.9-445.8 h^{-1}) than that of the previously reported Ag catalysts for hydrogenation of nitroaromatics (TOF=20-160 h^{-1}) [35-37]. The present catalyst system can also be extended facilely for the hydrogenation of various olefins. It has been found that the simple olefins and α,β-unsaturated ketones can be hydrogenated smoothly under the used condition (Table S1, entries 1-5), which all afford selectively the corresponding saturated C-C single-bond compounds despite of variable reactivity.

<Insert Table 3>

The recyclability of the catalysts is one of the most important aspects in the view of environmental and economics points in either research or industry [38]. As depicted in Fig. 9, the recyclability of Ag@C/ZrPP-500R catalyst was evaluated by choosing nitrobenzene as a model substrate under the optimal experimental conditions. After each run, the catalyst was separated by the simple filtration, washed with THF and reused in the next cycle. The conversion of nitrobenzene almost keeps unchanged in the first five run, but decreases slightly from 100% to 94% after the sixth run. The

Ag content in the spent catalyst after the sixth run has been determined by ICP, which is found to be 0.69 wt. %, actually very close to the initial 0.72 wt. %, indicating the leaching of Ag species on the present catalyst is negligible. Additionally, the spent Ag@C/ZrPP-500R catalyst actually shows the same XRD pattern as that of the fresh one (Fig. 1e and 1f), indicating the ZrPP is very stable and phase transformation does not happen. The diffraction peak of Ag species are also invisible, which implies that Ag particles exist still in a very small size and high dispersion. The SEM characterization shows that the morphology of the spent Ag@C/ZrPP-500R catalyst does not change (Fig. 4e and 4f). After the sixth run, the small-sized Ag cluster are still dispersed homogeneously on the ZrPP. The size of Ag cluster mainly ranges from 1.0-2.0 nm and the mean size is about 1.52 nm (Fig. S5a), almost identical to that of the fresh catalyst (1.43 nm), indicating that the immobilized Ag cluster in ZrPP is highly resistant to leaching and aggregation. The slight decrease in catalytic activity may be due to the carboneceous deposits on the surface of the catalyst from side-reaction [39].

< Insert Fig. 9>

It is well known that there are two main reaction routes for the hydrogenation of nitroaromatics under reducing conditions: direct and indirect. The direct route is reduction of nitro groups in aromatic ring to the nitroso, further to the hydroxylamine (two continuous steps) and the hydroxylamine is finally reduced to the amine. The indirect route is as follows, the intermediates of nitroso and hydroxylamine firstly condense to generate azo intermediates, which subsequently undergo hydrogenation and cleavage of the azo bond to produce aniline [40]. In the present catalytic system, when hydrogenation of nitrobenzene was chosen as a model reaction, there was only very small amount (in <3% selectivity) of phenylhydroxylamine as intermediate was detected in the products apart from aniline at the initial stage of reaction (20 min) and its selectivity declined eventually became zero. Azoxybenzene or azobenzene was not founded in the liquid products. Based on these results, the hydrogenation of

nitrobenzene to aniline occurs through the direct route instead of the indirect route on the present catalyst.

Fig. 10 shows the FT-IR spectra of the Ag catalysts after introducing nitrobenzene. When nitrobenzene is adsorbed on the catalyst, the asymmetric $\nu_{as}(NO_2)$ band for nitrobenzene appears at 1525 cm^{-1} (Fig.10a-10c), which is distinct from that of the pure nitrobenzene (1527 cm^{-1}) (Fig. 10d), suggesting that nitrobenzene interacts with the catalyst surface through the nitro group. The band at 1350 cm^{-1} attributing to the symmetric $\nu_{s}(NO_2)$ of nitrobenzene absorbed on the catalyst, remains actually the same as that of the pure nitrobenzene [41]. Since the introduction of Ag into ZrPP does not exert any effect on the asymmetric $\nu_{as}(NO_2)$ IR vibration (Fig. 10a-10c), suggesting that the nitro group of nitrobenzene is adsorbed preferentially on the ZrPP support and then is activated in the subsequent reaction. The Ag cluster on the ZrPP could play a vital role in H_2 dissociation, facilitating the active hydrogen atom to attack nitro group of nitroaromatics. Finally, the corresponding aromatic amines are generated.

< Insert Fig. 10>

From our previous research, it demonstrated that zirconium phosphate owned middle to strong Bronsted acid sites (surface hydroxyl groups) and Lewis acid sites (metal sites) [24,42]. An enhanced adsorption/activation of nitrobenzene can occur in the presence of these surface acid groups [43,44]. Meanwhile, nitrobenzene can still absorb on surface acid sites even in the presence of aniline, and at least partial displacement of aniline by nitrobenzene indeed happens [45]. As a result, the absorbed nitrobenzene is activated on the acid support. Next, H_2 is splitted into active hydrogen atoms on Ag cluster, and then transfers to the polar nitro group to generate a hydroxylamine intermediate as we have detected at the initial stage of reaction. The hydroxylamine intermediate undergoes a further hydrogenation to afford the final aniline product (Scheme 2).

<Insert Scheme 2>

5. Conclusions

We have developed an easy strategy to introduce the cationic Ag cluster into α-ZrP by a simple ion-exchange approach, and the sequential process of carbonization, calcination and reduction offered a uniform Ag cluster intercalated in ZrPP support. The characterization indicated that all resulting catalysts derived from α-ZrP also showed a layered structure and kept highly stable during the reaction. The as-prepared Ag@C/ZrPP-500R catalyst exhibits excellent activity and catalytic stability for the hydrogenation of a variety of nitroaromatics even if the loading of Ag was as low as 0.72 wt.% on the support. It was found that the thermal treatment is very critical for achieving high activity. The residual carbon layer is essential to protect the Ag cluster from agglomeration and sintering. The ZrPP plays an important role not only in stabilizing Ag cluster, but also in absorbing nitroaromatics during the reaction. The combination of zirconium phosphate and other cationic clusters can be definitely applied for the stabilization of metal NCs, and accelerate research in the area of hydrogenation catalysis and allows us to design a robust metal NCs catalyst resistant to leaching and aggregation.

Acknowledgements

The authors are grateful for support from the National Natural Science Foundation of China (21373082, 21773061), the innovation Program of Shanghai Municipal Education Commission (15ZZ031), and the Natural Science Foundation of Shanghai (16ZR1409500).

References

[1] P.L. Xavier, K. Chaudhari, A. Baksi, T. Pradeep, Nano Rev. 3 (2012) 14767–14782.

[2] A. Chandrasekar, T. Pradeep, J. Phys. Chem. C 116 (2012) 14057–14061.

[3] Y. Tan, X.Y. Liu, L.L. Zhang, A.Q. Wang, L. Li, X.L. Pan, S. Miao, M. Haruta,

H.S. Wei, H. Wang, F.J. Wang, X.D. Wan, T. Zhang, Angew. Chem. Int. Ed. 56 (2017) 2709–2713.

[4] R.C. Jin, C.J. Zeng, M. Zhou, Y.X. Chen, Chem. Rev. 116 (2016) 10346–10413.

[5] I. Chakraborty, T. Pradeep, Chem. Rev. 117 (2017) 8208–8271.

[6] L.H. Liu, A. Corma, Chem. Rev. 118 (2018) 4981–5079.

[7] T. Takei, Y.J. Kobayashi, H. Hata, Y. Yonesaki, N. Kumada, N. Kinomura, T.E. Mallouk, J. Am. Chem. Soc. 128 (2006) 16634–16640.

[8] W.J. Mu, Q.H. Yu, R. Zhang, X.X. Li, R. Hu, Y. He, H.Y. Wei, Y. Jian, Y.C. Yang, J. Mater. Chem. A 5 (2017) 24388–24395.

[9] H.N. Kim, S.W. Keller, T.E. Mallouk, J. Schmitt, G. Decher, Chem. Mater. 9 (1997) 1414–1421.

[10] M.R. Duff, C.V. Kumar, J. Phys. Chem. B 113 (2009) 15083–15089.

[11] W.Y. Xing, G.X. Jie, L. Song, X. Wang, X. Lv, Y. Hu, Mater. Chem. Phys. 125 (2011) 196–201.

[12] M. Pica, M. Nocchetti, B. Ridolfi, A. Donnadio, F. Costantino, P.L. Gentili, M. Casciola, J. Mater. Chem. A 3 (2015) 5525–5534.

[13] M.Q. Shen, Y. Zhang, J.Q. Wang, C. Wang, J. Wang, J. Catal. 358 (2018) 277–286.

[14] M. Qu, H. Li, L.H. Xie, S.T. Yan, J.R. Li, J.H. Wang, C.Y. Wei, Y.W. Wu, X.M. Zhang, J. Am. Chem. Soc. 139 (2017) 12346–12349.

[15] Y. Hu, Y.Y. Yu, X.G. Zhao, H.M. Yang, B. Feng, H. Li, Y.X. Qiao, L. Hua, Z.Y. Pan, Z.S. Hou, Sci. Chi. Chem. 53 (2010) 1541–1548.

[16] Y.Y. Yu, W.W. Zhu, L. Hua, H.M. Yang, Y.X. Qiao, R. Zhang, L. Guo, X.G. Zhao, Z.S. Hou, J. Colloid Interf. Sci. 415 (2014) 117–126.

[17] Z.P. Dong, X.D. Le, C.X. Dong, W. Zhang, X.L. Li, J.T. Ma, Appl. Catal. B 162 (2015) 372–380.

[18] J.J. Mao, W.X. Chen, W.M. Sun, Z. Chen, J.J. Pei, D.S. He, C.L. Lv, D.S. Wang, Y.D. Li, Angew. Chem. Int. Ed. 56 (2017) 11971–11975.

[19] Q.H. Wei, Q.X. Ma, P.P. Zuo, H. Fan, S. Qu, W.Z. Shen, ChemCatChem 10 (2018) 1019–1026.

[20] M. Cinelli, S.R. Coles, M.N. Nadagouda, J. Błaszczyński, R. Słowiński, R.S. Varma, K. Kirwan, Green Chem. 17 (2015) 2825–2839.

[21] B.G. Alberti, M. Casciola, U. Costantino, R. Vivani, Adv. Mater. 8 (1996) 291–303.

[22] M. Santiago–Berríos, C. Declet–Flores, A. David, S. Borrero, M.M. Velez, A. Diaz–Diaz, A.R. Guadalupe, J.L. Colon, Langmuir 28 (2012) 4447–4452.

[23] International Centre of Diffraction Date (ICDD), PCPDF 36–0188.

[24] H.M Gan, X.G. Zhao, B.N. Song, L. Guo, R. Zhang, C. Chen, J.Z. Chen, W.W. Zhu, Z.S. Hou, Chin. J. Catal. 35 (2014) 1148–1156.

[25] I. Bouali, E. Rocca, D. Veys–Renaux, B. Rhouta, A. Khalil, A.A. Aghzzaf, Appl. Surf. Sci. 422 (2017) 778–786.

[26] D.J. MacLachlan1, K.R. Morgan, J. Phys. Chem. 96 (1992) 3458–3464.

[27] R. Weingarten, Y.K. Kim, G.A. Tompsett, A. Fernández, K.S. Han, E.W. Hagaman, W.C.C. Jr, J.A. Dumesic, G.W. Huber, J. Catal. 304 (2013) 123–134.

[28] M.S.P. Francisco, W.S. Cardoso, Y. Gushikem, Langmuir 20 (2004) 8707–8714.

[29] L.L. Sun, D.Y. Zhang, Y.M. Sun, S.Y. Wang, J. Cai, Adv. Funct. Mater. 28 (2018) 1707231.

[30] F. Wang, J.Z. Ma, G.Z. He, M. Chen, C.B. Zhang, H. He, ACS Catal. 8 (2018) 2670–2682.

[31] C. Kumara, H.M. Luo, D.N. Leonard, H.M. Meyer, J. Qu, ACS Appl. Mater. Interfaces 9 (2017) 37227–37237.

[32] L.G. Moura，M.V.O. Moutinho, P. Venezuela, F. Mauri, A. Righi, M.S. Strano, C. Fantini, M.A. Pimenta, Carbon 117 (2017) 41–45.

[33] S.R. Khan, Z.H. Farooqi, W. Zaman, A. Ali, R. Begum, F. Kanwal, M. Siddiq, Mater. Chem. Phys. 171 (2016) 318–327.

[34] J.H. Wang, Z.L. Yuan, R.F. Nie, Z.Y. Hou, X.M. Zheng, Ind. Eng. Chem. Res. 49 (2010) 4664–4669.

[35] A.K. Patra, N.T. Vo, D. Kim, Appl. Catal. A 538 (2017) 148–156.

[36] W. Feng, T.T. Huang, L.Q. Gao, X.F. Yang, W.B. Deng, R. Zhou, H.J. Liu, RSC Adv. 8 (2018) 6288–6292.

[37] H. Mao, C.G. Ji, M.H. Liu, Z.Q. Cao, D.Y. Sun, Z.Q. Xing, X. Chen, Y. Zhang, X.M. Song, Appl. Surf. Sci. 434 (2018) 522–533.

[38] C. Jiang, Z. Shang, X. Liang, ACS Catal. 5 (2015) 4814–4818.

[39] W.W. Lin, H.Y. Cheng, J. Ming, Y.C. Yu, F.Y. Zhao, J. Catal. 291 (2012) 149–154.

[40] X.X. Shi, X.G. Wang, X.F. Shang, X.J. Zou, W.Z. Ding, X.G. Lu, ChemCatChem 9 (2017) 3743–3751.

[41] K. Shimizu, Y. Miyamoto, A. Satsuma, J. Catal. 270 (2010) 86–94.

[42] W. Ni, D. Li, X. Zhao, W. Ma, K. Kong, Q. Gu, M. Chen, Z. Hou, Catal. Today 319 (2019) 66–75.

[43] A. Nieto-Marquez, S. Gil, A. Romero, J.L. Valverde, S. Gomez-Quero, M.A. Keane, Appl. Catal. A: Gen. 363 (2009) 188–198.

[44] K. Shimizu, Y. Miyamoto,T. Kawasaki, T. Tanji, Y. Tai, A. Satsuma, J. Phys. Chem. C 113 (2009), 17803–17810.

[45] U. Hartfelder, C. Kartusch, J. Sa, J.A. van Bokhoven, Catal. Commun. 27 (2012) 83–87.

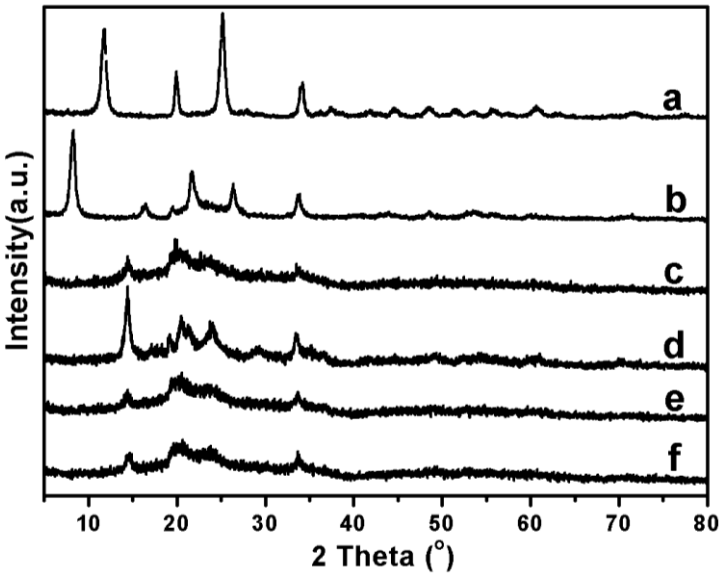

Fig. 1. XRD patterns of (a) α-ZrP, (b) Ag/α-ZrP, (c) Ag@C/ZrPP, (d) Ag@C/ZrPP-500, (e) Ag@C/ZrPP-500R, and (f) the spent Ag@C/ZrPP-500R catalysts.

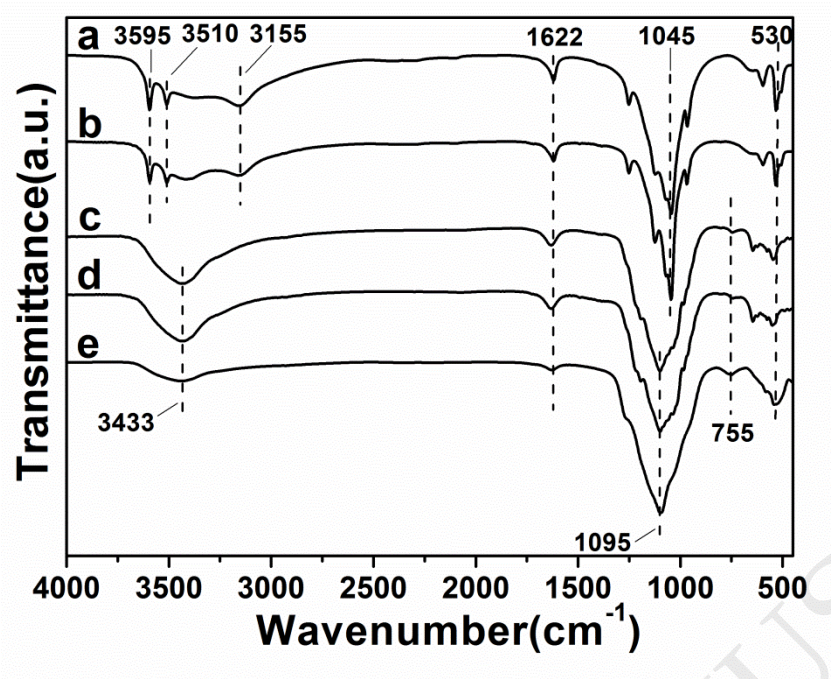

Fig. 2. FT–IR spectra of (a) α-ZrP, (b) Ag/α-ZrP, (c) Ag@C/ZrPP, (d) Ag@C/ZrPP-500, and (e) Ag@C/ZrPP-500R catalysts.

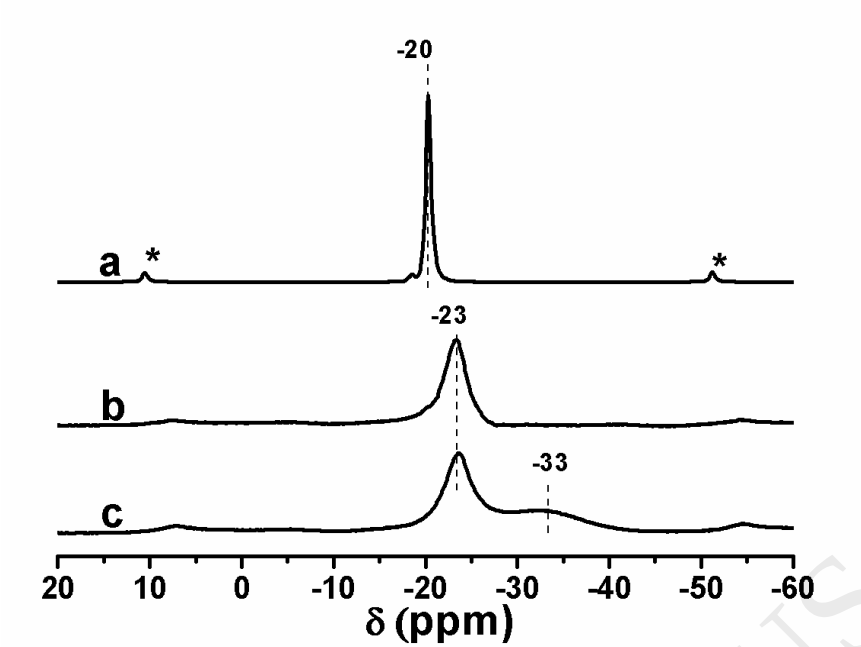

Fig. 3. Solid–state ^{31}P MAS NMR spectrum (shifts relative to H_3PO_4) of (a) α-ZrP, (b) Ag/α-ZrP, and (c) Ag@C/ZrPP-500R catalysts. Peaks marked with * are rotation bands.

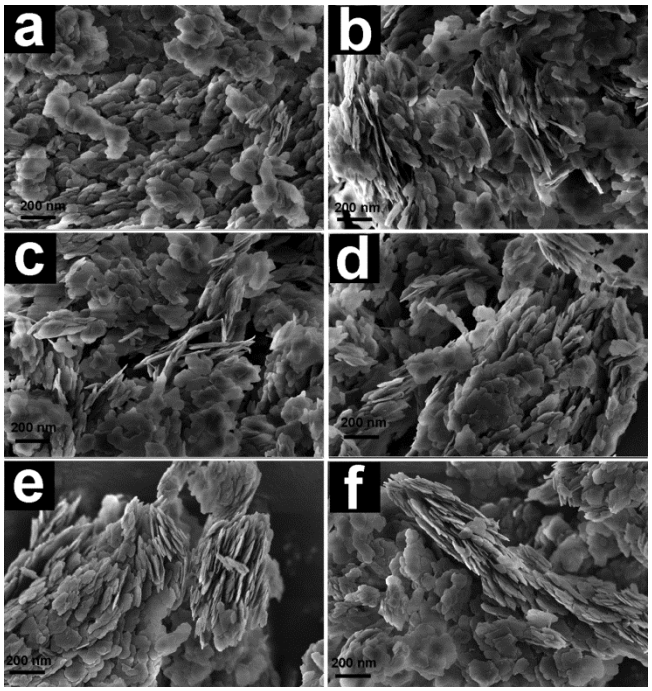

Fig. 4. The SEM images of (a) α-ZrP, (b) Ag/α-ZrP, (c) Ag@C/ZrPP, (d) Ag@C/ZrPP-500, (e) Ag@C/ZrPP-500R, and (f) the spent Ag@C/ZrPP-500R catalysts. The scale bar is 200 nm.

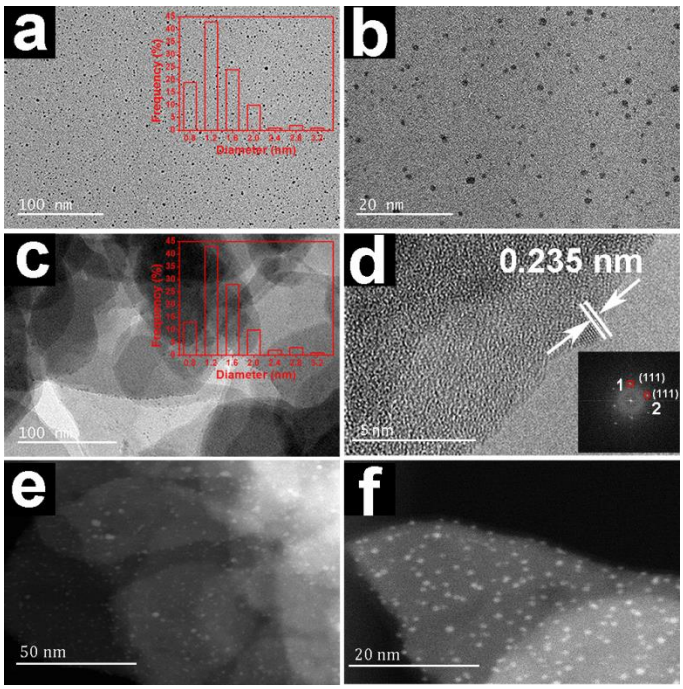

Fig. 5. HRTEM images of Ag_{74} cluster precursor (a, b), Ag@C/ZrPP-500R at different magnification and determination of the interplanar spacings by FFT(c,d), and HAADF-STEM images of Ag@C/ZrPP-500R catalyst (e, f).

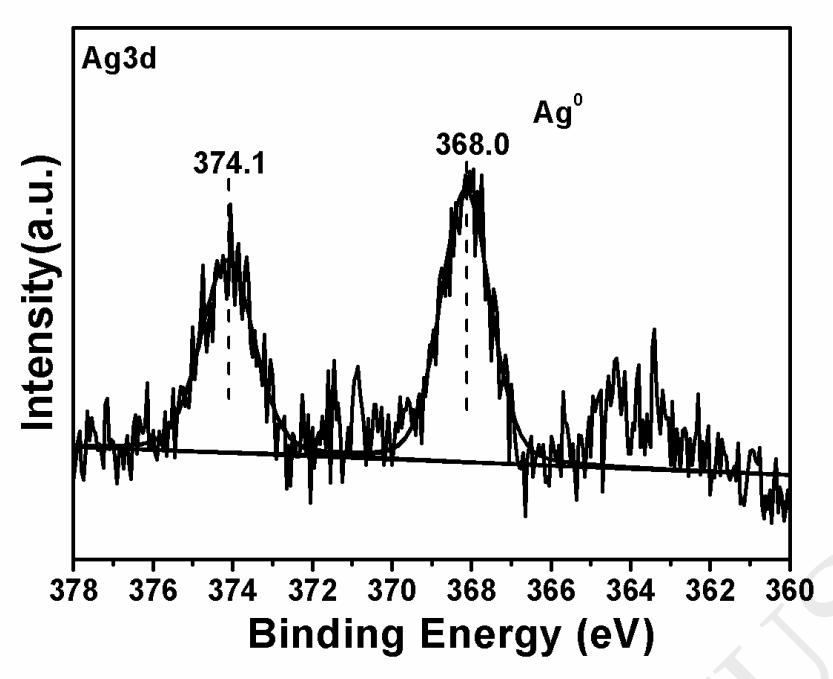

Fig. 6. Ag 3d X–ray photoelectropy spectroscopy (XPS) spectrum of the Ag@C/ZrPP-500R catalyst.

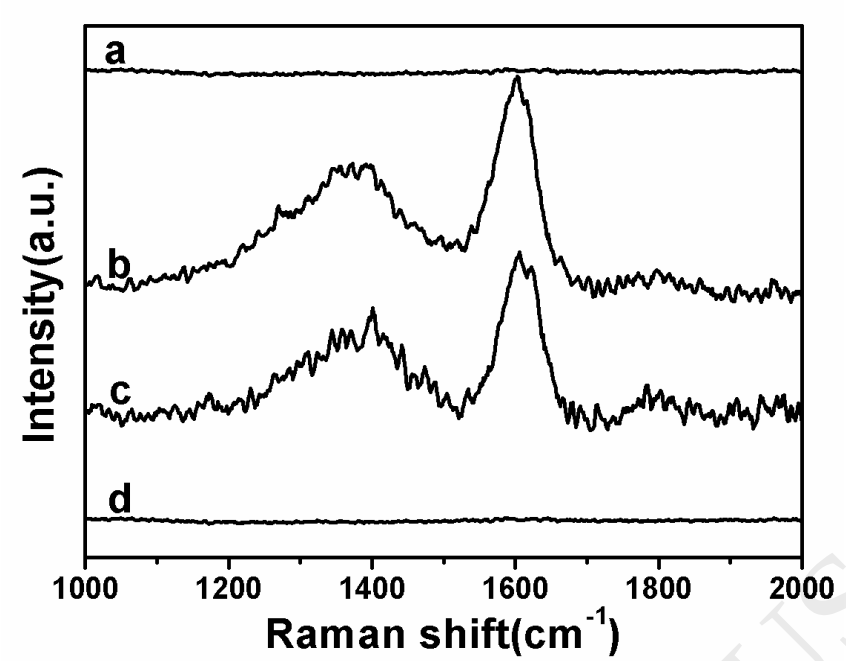

Fig. 7. The Raman spectroscopy of the catalysts. (a) ZrPP, (b) Ag@C/ZrPP, (c) Ag@C/ZrPP-500R, and (d) Ag@C/ZrPP-550R.

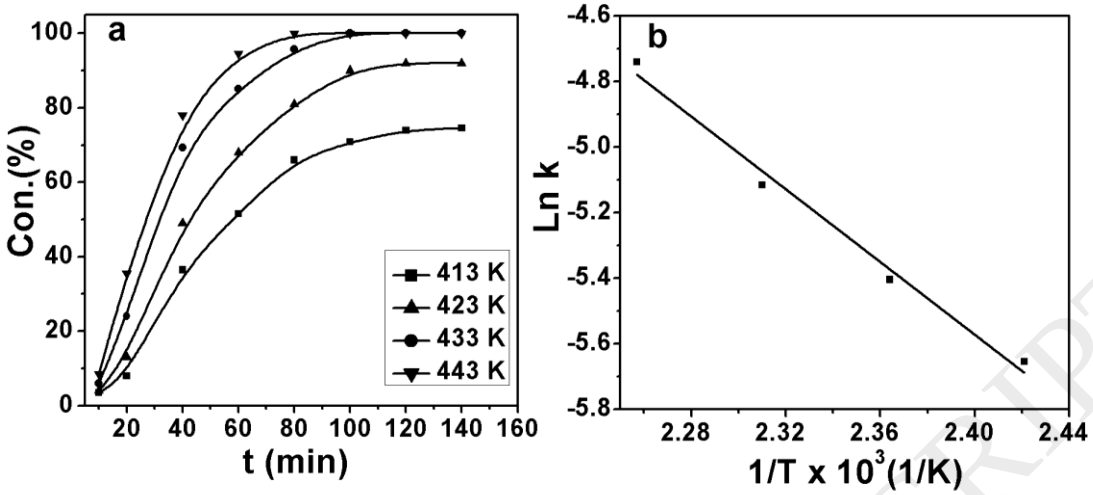

Fig. 8. Conversion/time profiles of hydrogenation reactions catalyzed by Ag@C/ZrPP-500R at different temperatures. Arrhenius plots for the hydrogenation reaction of Ag@C/ZrPP-500R. The observed rate constants (k) were calculated with the initial rates at different temperatures. 4 MPa H_2 pressure, 50 mg catalyst, 1.5 mmol substrate, 5 mL solvent (THF), 160 ^{o}C, 1.5 h, stirring rate (1000 rpm).

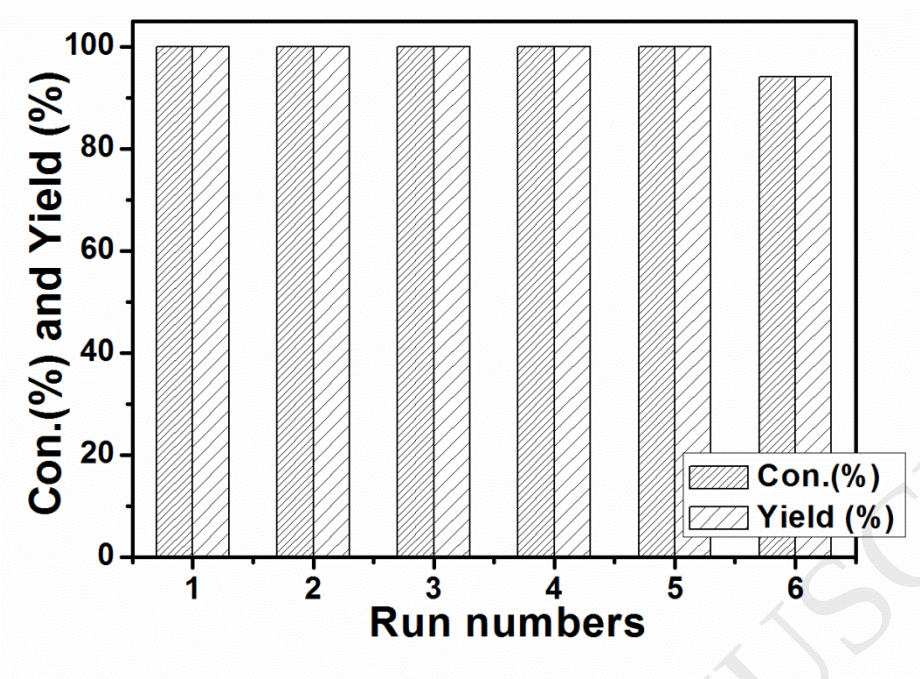

Fig. 9. The recycibility of Ag@C/ZrPP-500R catalyst for selective hydrogenation of nitrobenzene.

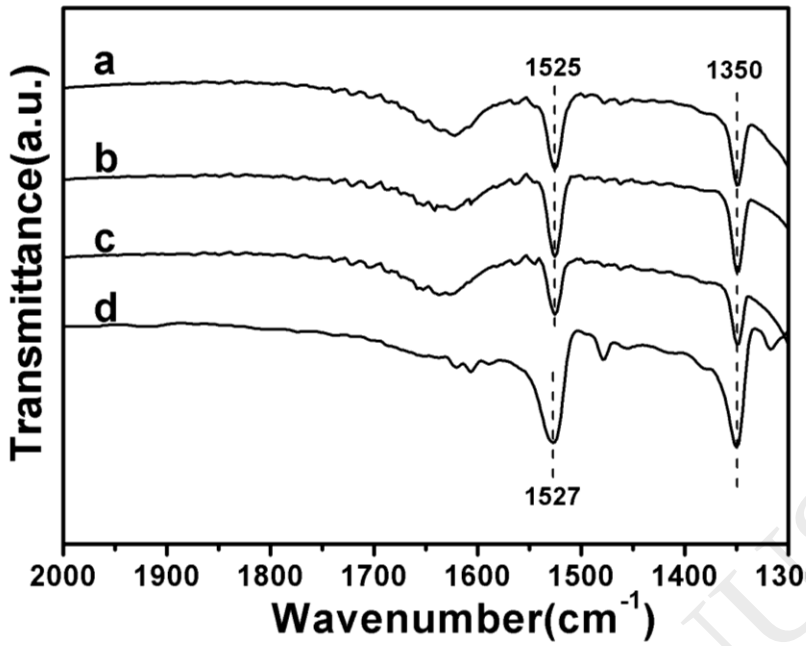

Fig. 10. FT-IR spectra of adsorbed nitrobenzene on different catalysts. (a) ZrPP, (b) Ag@C/ZrPP, (c) Ag@C/ZrPP-500R, and (d) nitrobenzene, and (a–c) introduced nitrobenzene (3.0 mmol g^{-1}), followed by drying under the vacuum for 1 h at 40 ^{o}C.

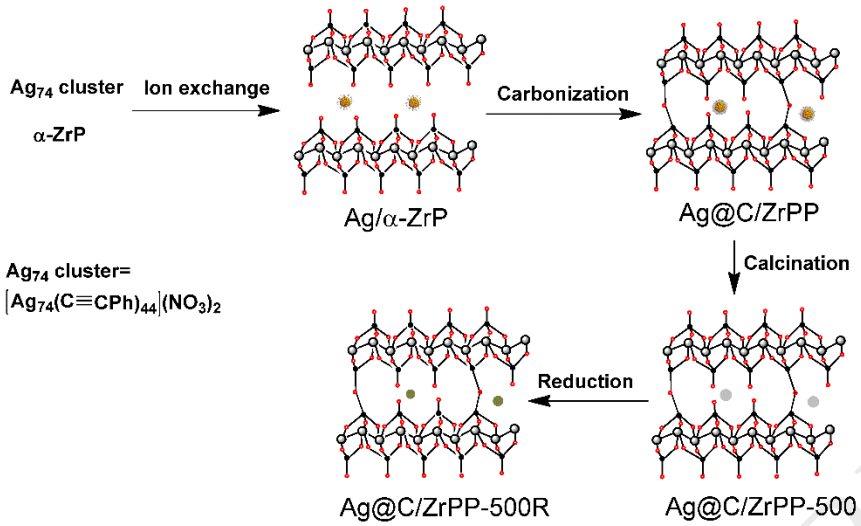

Scheme 1. The preparation route of the Ag NC catalysts.

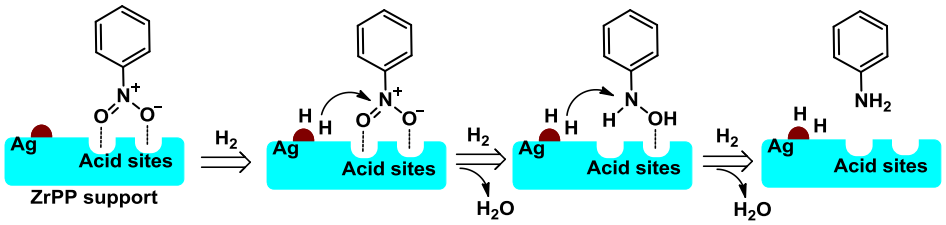

Scheme 2. Proposed mechanism for the nitrobenzene hydrogenation on Ag@C/ZrPP-500R catalyst.

Table 1. Porosity properties of the catalysts.

Entries	Sample	S_{BET}[a] ($m^2\ g^{-1}$)	V_{total}[b] ($cm^3\ g^{-1}$)	Pore size[c] (nm)
1	α-ZrP	45.5	0.27	10.5
2	Ag/α-ZrP	41.5	0.24	11.5
3	Ag@C/ZrPP	41.2	0.25	11.2
4	Ag@C/ZrPP-500	40.5	0.24	12.0
5	Ag@C/ZrPP-500R	40.9	0.23	11.8

[a] Surface area were calculated from the nitrogen adsorption isotherm using the BET method. [b] Total pore volume was calculated from nitrogen sorption isotherms at P/P_0 = 0.99. [c] Pore size was calculated by the BJH method.

Table 2. Catalytic performances for hydrogenation of nitrobenzene by the different catalysts [a]

Entries	Catalysts	Con.(%)	Yield (%)
1	no catalysts	0	0
2	Ag cluster	5	5
3	α-ZrP	0	0
4	ZrPP	0	0
5	Ag/α-ZrP	7.5	7.5
6	Ag@C/ZrPP	<1	<1
7	Ag@C/ZrPP-400R	67.5	67.5
8	Ag@C/ZrPP-500R	100	100
9	Ag@C/ZrPP-550R	44.5	44.5

[a] Reaction condition: 4 MPa H_2 pressure, 160 ^oC, 50 mg catalyst, 1.5 mmol nitrobenzene, stirring rate, 1000 rpm, 1.5 h, 5 mL solvent (THF).

Table 3. Hydrogenation of various nitroaromatics over Ag@C/ZrPP-500R catalyst [a]

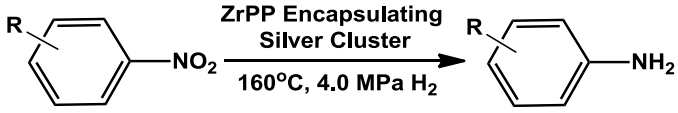

Entry	T (h)	R–	Yield (%)	TOF (h^{-1})
1	1.5	H	100.0	297.2
2	1.5	*p*–Cl	99.5	297.2
3	1.5	*p*–methyl	100.0	297.2
4	1.0	*p*–methoxy	100.0	445.8
5	1.0	*p*–hydroxyl	100.0	445.8
6	1.5	*o*–hydroxyl	100.0	297.2
7	1.5	*p*–amino	100.0	297.2
8	2.0	*m*–acetyl	96.5	222.9
9	1.5	*p*–acetyl	94.5	297.2

[a] Reaction conditions unless otherwise noted: 4 MPa H_2 pressure, 50 mg catalyst, 1.5 mmol substrate, 5 mL solvent (THF), 160 °C, stirring rate, 1000 rpm, 1.5 h. The conversion of the substrates all reached 100%.